

Potentials of thin film silicon anodes in soft solid state batteries

Julian Brokmann^{a,b}, Han-Pin Hsieh^c, Ann-Sophie Gail^a, Matteo Kaminski^{a,b}, Nikolas Dilger^a,
Sebastian Melzig^{a,b}, Fu-Ming Wang^c, Sabrina Zellmer^{a,b}

- Fraunhofer Institute for Surface Engineering and Thin Films IST, Riedenkamp 2, Braunschweig 38108, Germany. E-Mail: sabrina.zellmer@ist.fraunhofer.de
- Technische Universität Braunschweig, Institute for Particle Technology, Volkmaroder Straße 5, Braunschweig 38104, Germany. E-Mail: s.zellmer@tu-braunschweig.de
- National Taiwan University of Science and Technology, Graduate Institute of Applied Science and Technology, No.43 Keelung Rd., Sec. 4, Da'an Dist., Taipei City 106335, Taiwan (R.O.C.). E-Mail: mccabe@mail.ntust.edu.tw

Table S1: Quantitative compositional analysis using electron probe microanalysis (EPMA)

	<u>Si</u>	<u>O</u>
200 nm Si@Cu	43,9 at%	56,1 at%
1000 nm Si@Cu	52,6 at%	47,4 at%
2000 nm Si@Cu	52,1 at%	47,9 at%

The X-ray diffraction pattern of the silicon film after lithiation is shown in Fig. S2 in the 2θ range from 10° to 80° . The diffractogram is characterized by a broad diffuse feature between approximately 15° and 30° (2θ), indicative of an amorphous structure and attributed to lithiated silicon (Li_xSi). Compared to the pristine state, the increased intensity of this halo suggests the formation of an amorphous alloy upon lithiation. Overlaid on this amorphous background, sharp reflections are observed at approximately 43° , 50° , and 74° , corresponding to the (111), (200) and (220) planes of the copper current collector. These reflections dominate the diffractogram due to the high crystallinity and thickness of the substrate relative to the silicon thin film.

After lithiation, an increased intensity is observed in the region around $43\text{--}44^\circ$, which coincides with the Cu (111) reflection and is attributed to changes in the effective scattering conditions of the substrate, such as variations in film density, surface roughness, or X-ray penetration depth induced by lithiation. No additional distinct reflections that could be assigned to crystalline lithium silicide phases are detected within the measured angular range. In particular, no evidence for the formation of crystalline $\text{Li}_{15}\text{Si}_4$ is observed, indicating that the lithiated silicon remains predominantly amorphous under the investigated conditions.

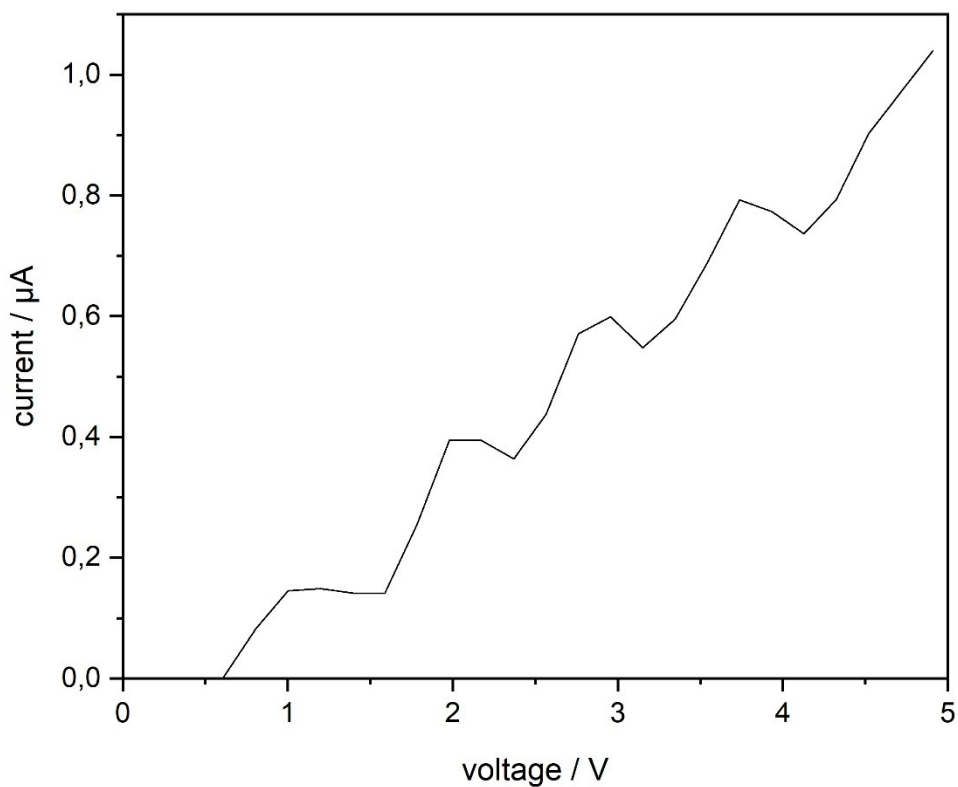


Figure S1: LSV curves of CEAM950 organic polymer solid-state electrolyte

To measure the ionic conductivity, the CEAM950 sample was poured into a custom Teflon cell equipped with stainless steel working and counter electrodes. Impedance spectra were recorded four times at a constant temperature of 60 °C. Based on the average values of these four measurements, the ionic conductivity was determined to be $3.41 \cdot 10^{-5}$ S/cm.

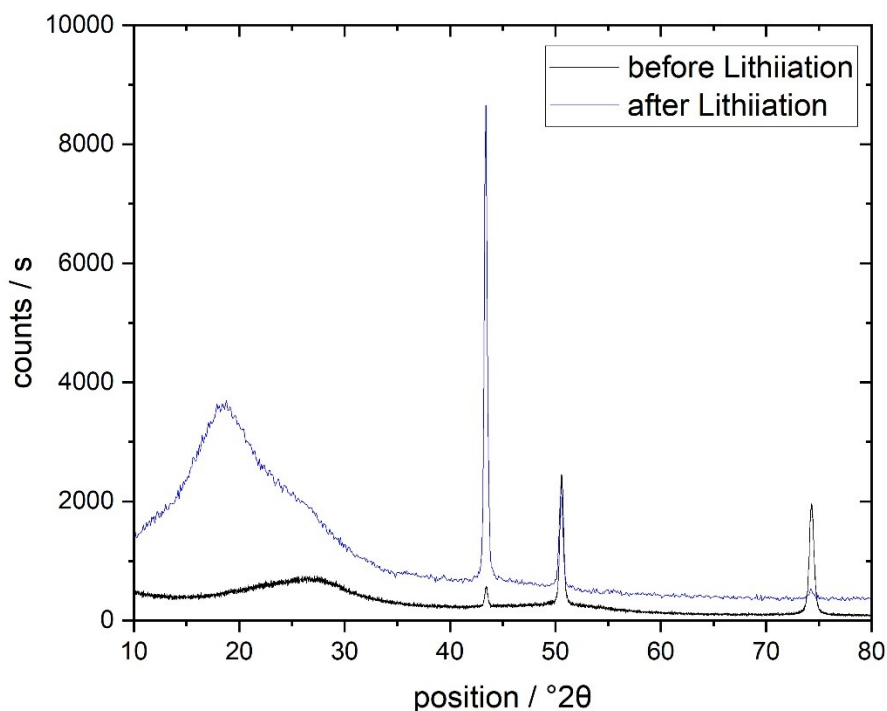


Figure S2: X-ray diffraction patterns of the sputter-deposited silicon film on a copper substrate before and after lithiation in the 2θ range from 10° to 80° . The patterns exhibit a broad diffuse feature between approximately 15° and 30° (2θ), associated with amorphous Si and Li_xSi , as well as sharp reflections at around 43° , 50° and 74° , corresponding to the Cu current collector. No additional distinct reflections attributable to crystalline lithium silicide phases are observed after lithiation.

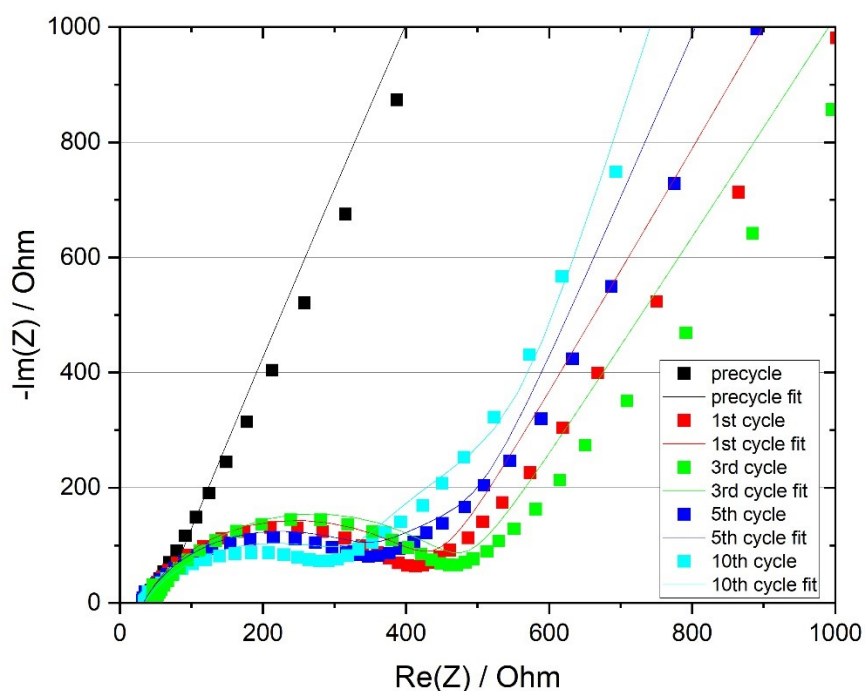


Figure S3: Electrochemical impedance spectra (Nyquist plots) of the 200 nm Si@Cu electrode at different cycle numbers (pre-cycle, 1st, 3rd, 5th and 10th cycle) including corresponding equivalent circuit fits. The spectra are consistently described using the circuit $R_0-p(R_1, \text{CPE}_1)-p(R_2, \text{CPE}_2)-R_3-\text{CPE}_3$ over all cycles. The stable circuit topology reflects that the dominant electrochemical processes remain qualitatively unchanged during cycling, while the evolution of the spectra is captured by gradual changes in the interfacial contributions.

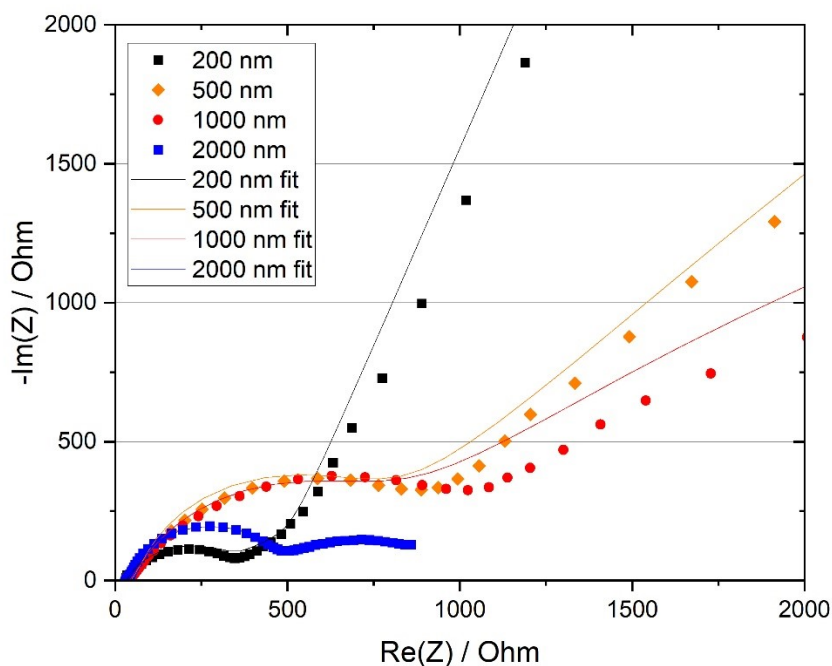


Figure S4: Electrochemical impedance spectra (Nyquist plots) of Si@Cu electrodes with varying silicon thickness (200 nm, 500 nm, 1000 nm and 2000 nm) after the 5th cycle, including corresponding equivalent circuit fits. The 200 nm and 500 nm electrodes are described using the circuit $R_0-p(R_1,CPE_1)-p(R_2,CPE_2)-R_3-CPE_3$, whereas the 1000 nm and 2000 nm electrodes require the inclusion of a Warburg element ($R_0-p(R_1,CPE_1)-p(R_2,CPE_2)-W_{01}$). The change in circuit topology reflects the increasing importance of transport limitations and the deviation from a homogeneous thin-film response at higher thicknesses.

Equivalent circuit analysis and scope of interpretation

The impedance spectra were fitted using equivalent circuit models to support the qualitative interpretation presented in the main text. The corresponding fits are shown in Fig. S3 (cycle-dependent comparison for 200 nm) and Fig. S4 (thickness-dependent comparison).

For the 200 nm Si@Cu electrode, the circuit

$$R_0-p(R_1,CPE_1)-p(R_2,CPE_2)-R_3-CPE_3$$

provides a consistent description of the impedance response over all investigated cycles. Since the circuit topology remains unchanged, the fitted parameters can be qualitatively compared. The evolution of the spectra is reflected in gradual changes of the interfacial elements, consistent with progressive interphase formation and increasing surface heterogeneity. However, even in this case, the parameters should be interpreted with caution, as constant phase elements represent distributed processes rather than ideal capacitive behaviour.

In the thickness-dependent comparison, two different circuit topologies are required. The 200 nm and 500 nm electrodes are described by

$$R_0-p(R_1,CPE_1)-p(R_2,CPE_2)-R_3-CPE_3,$$

whereas the 1000 nm and 2000 nm electrodes require

$$R_0-p(R_1,CPE_1)-p(R_2,CPE_2)-W_{01}.$$

The introduction of a Warburg-type element reflects the increasing importance of lithium transport limitations with increasing film thickness. At the same time, the impedance response of the thickest films deviates from ideal diffusion behaviour, indicating non-uniform current distribution and spatially heterogeneous transport pathways. As a consequence, the fitted parameters cannot be uniquely assigned

to well-defined physical processes across all thicknesses. In particular, for the 1000 nm and 2000 nm electrodes, the extracted values represent effective parameters of a structurally evolving system rather than intrinsic material properties. Therefore, the equivalent circuit analysis is used to identify dominant processes and regime changes, rather than to provide a strictly quantitative comparison of individual fit parameters across all samples.